

# Highly Efficient Three Primary Color Organic Single-Crystal Light-Emitting Devices with Balanced Carrier Injection and Transport

Ran Ding, Jing Feng,\* Feng-Xi Dong, Wei Zhou, Yang Liu, Xu-Lin Zhang, Xue-Peng Wang, Hong-Hua Fang, Bin Xu, Xian-Bin Li, Hai-Yu Wang, Shu Hotta, and Hong-Bo Sun\*

Organic single crystals have a great potential in the field of organic optoelectronics because of their advantages of high carrier mobility and high thermal stability. However, the application of the organic single crystals in light-emitting devices (OLEDs) has been limited by single-layered structure with unbalanced carrier injection and transport. Here, fabrication of a multilayered-structure crystal-based OLED constitutes a major step toward balanced carrier injection and transport by introducing an anodic buffer layer and electron transport layer into the device structure. Three primary color single-crystal-based OLEDs based on the multilayered structure and molecular doping exhibit a maximum luminance and current efficiency of  $820 \text{ cd cm}^{-2}$  and  $0.9 \text{ cd A}^{-1}$ , respectively, which are the highest performance to date for organic single-crystal-based OLEDs. This work paves the way toward high-performance organic optoelectronic devices based on the organic single crystals.

of their great varieties and high emission efficiency. However, the problem of low carrier mobility and disordered structure in amorphous materials still exists accompanying with the development and deeply influences the performance of OLEDs. So as to further improve the performance of OLEDs, researchers turn their attention to organic single crystals which possess the superior properties of thermal stability, higher carrier mobility, and high emission efficiency with light amplification ability due to their lower content of impurity and highly ordered molecule arrangement compared to amorphous materials. And their inherent long-range structural ordering could effectively avoid exciton quenching under high current density. Some emissive molecule-based organic single crystals demonstrate a rather low

threshold for light amplification under optical pumping. For these important benefits, organic single crystals have been widely investigated in the field of optoelectronic devices such as optically pumped lasers, organic field-effect transistors (OFETs), organic light-emitting field-effect transistors (OLEFETs), and OLEDs.<sup>[11–17]</sup> In previous reports, the single crystal mobility for pentacene is up to  $1.4 \text{ cm}^2 \text{ V}^{-1} \text{ s}^{-1}$  which is comparable to the value for amorphous hydrogenated silicon.<sup>[16]</sup> And the single crystals of rubrene have reached a maximum mobility of about  $43 \text{ cm}^2 \text{ V}^{-1} \text{ s}^{-1}$ , which is at least two orders of magnitude higher than amorphous materials.<sup>[17]</sup> A relatively low optically pumped

## 1. Introduction

In the past three decades, great progress has been made in the field of organic light-emitting devices (OLEDs). They are increasingly used in the commercial flat-panel display and solid-state lighting owing to their remarkable performance, such as high energy efficiency, vibrant colors, fast refresh rate, mechanical flexibility, and so on.<sup>[1–9]</sup> Since Tang and VanSlyke fabricated the first high efficiency thin-film OLEDs by vacuum deposition method in 1987,<sup>[10]</sup> organic amorphous semiconductor materials have been extensively investigated because

Dr. R. Ding, Prof. J. Feng, F.-X. Dong, W. Zhou, Dr. X.-L. Zhang, X.-P. Wang, Dr. H.-H. Fang, Prof. X.-B. Li, Prof. H.-Y. Wang, Prof. H.-B. Sun  
State Key Laboratory on Integrated Optoelectronics  
College of Electronic Science and Engineering  
Jilin University  
2699 Qianjin Street, Changchun 130012, China  
E-mail: jingfeng@jlu.edu.cn; hbsun@jlu.edu.cn  
Dr. R. Ding  
International Research Centre for Nano Handling and Manufacturing of China (CNM)  
Changchun University of Science and Technology  
Changchun 130022, China

Y. Liu, Prof. B. Xu  
State Key Laboratory of Supermolecular Structures and Materials  
Jilin University  
2699 Qianjin Street, Changchun 130012, China  
Prof. S. Hotta  
Department of Macromolecular Science and Engineering  
Graduate School of Science and Technology  
Kyoto Institute of Technology  
Matsugasaki, Sakyo-ku, Kyoto 606-8585, Japan  
Prof. H.-B. Sun  
College of Physics  
Jilin University  
2699 Qianjin Street, Changchun 130012, China



DOI: 10.1002/adfm.201604659

amplified spontaneous emission threshold of  $8 \mu\text{J cm}^{-2}$  is reported from  $\alpha,\omega$ -di(biphenyl)-terthiophene (BP3T) single crystal.<sup>[15]</sup> Such single-crystal materials seem to be a promising candidate for high-performance OLEDs and electrically driven organic lasers, however, they still meet with a large amount of problems in application of devices.<sup>[18–21]</sup>

Despite its strong potential as active layer, the practical application of organic single crystals has been limited by their intrinsic properties, such as fragility, softness, and solubility in organic solvents, which are not appropriate for the conventional fabrication methods of vacuum-evaporation and solution-processing. In previous work, Li and Nakanotani fabricated single-crystal-based OLEDs with low light emission and inhomogeneous electroluminescence (EL) by simple lamination method to satisfy the intrinsic properties of organic single crystals.<sup>[19,20]</sup> But, the contact between crystal and electrodes determined by weak van der Waals forces would lead to poor connection and carrier injection. Very recently, we applied a simple and nondestructive method of template stripping to solve this problem, uniform light-emitting single-crystal-based OLEDs and a maximum luminance of  $16.87 \text{ cd m}^{-2}$  can be realized with improved contact between crystal and electrodes.<sup>[22]</sup> Then, the obtained polarized EL emission and polarization-induced color tunability from OLEDs based on BP3T single crystals were considered as an advantage for electrically driven organic lasers.<sup>[23]</sup> However, the efficiency of these single-crystal-based OLEDs is still quite low, compared to the conventional amorphous film OLEDs. Unbalanced carrier transport due to the different carrier mobilities in organic single crystals results in the recombination zone more close to the electrode; additionally, the mismatched work function causes the inefficient and unbalanced carrier injection. In order to achieve practical single-crystal-based OLEDs, the multilayered structure with electrode modification and carrier transport layers seems a remarkable method to improve charge carrier balance and EL external quantum efficiency (EQE). However, the fabrication of the multilayered structure in single-crystal-based OLEDs gives rise to the major technological challenge.

In this work, we demonstrate the multilayered structure in single-crystal-based OLEDs with anodic interfacial modification and electron-transport layers to enhance charge injection and balance hole and electron in recombination zone by employing the template stripping method. The devices exhibit a significantly lower turn-on voltage and higher emission efficiency. Molecular doping technique is used to realize three primary color light emissions in the multilayered single-crystal-based OLEDs. A pure blue single crystal 1,4-bis(4-methylstyryl)benzene (BSB-Me) is used as a host matrix, tetracene (Te) and pentacene (Pe) are used as guest materials, respectively. Efficient energy transfer occurs from BSB-Me as a donor to Te and Pe as acceptors through dipole–dipole interaction, resulting in tunable light emission from blue to green and red. The EL luminance and current efficiency of  $820 \text{ cd cm}^{-2}$  and  $0.9 \text{ cd A}^{-1}$  have been obtained, which are the highest performance reported up to now for organic single-crystal-based OLEDs. These results demonstrate the great potential of organic single crystals for use in a wide variety of high-performance organic optoelectronic devices, such as solid-state lighting, flat panel display, and electrically driven organic lasers.

## 2. Results and Discussion

### 2.1. Photoluminescence (PL) Characteristics of the Organic Single Crystal

The organic powders, BSB-Me, Te, and Pe have been purchased as host and guest materials without further purification in the fabrication. Their chemical structures are shown in **Figure 1a**. Before crystal growth, the uniform BSB-Me:Te and BSB-Me:Pe powders are prepared by milling the tetracene (or pentacene) and BSB-Me (2 and 25 mg, respectively) together in a mortar for a few minutes. Then, organic single crystals are grown by physical vapor transport method using the doped powders. Thin slice shaped crystals of pure BSB-Me, BSB-Me:Te, and BSB-Me:Pe at the dosage concentration of 8%, emitting blue, green, and red PL, are shown in the top-view photographs by fluorescence microscopy (**Figure 1b**). The crystals show a typical thickness of less than 400 nm and a length of several millimeters. The thinnest crystal employed in the single-crystal-based OLEDs is about 206 nm. **Figure S1a** (Supporting Information) shows the atomic force microscope (AFM) image of the thickness. The limitations of the crystal growth are dominated by the millimeter-scale and the transfer of crystal (see the Experimental Section). And the AFM images shown in **Figure S1b–d** (Supporting Information) reveal the surface morphology of pure BSB-Me, BSB-Me:Te, and BSB-Me:Pe crystals. The root mean square roughness of the crystals are 0.158 nm for pure BSB-Me, 0.169 nm for BSB-Me:Te, and 0.183 nm for BSB-Me:Pe, respectively. The crystal surfaces are smooth enough to fabricate single-crystal-based OLEDs with little leakage current. The PL spectra of doped and undoped crystals are measured under excitation of a 405 nm laser, and tetracene and pentacene are dissolved in tetrahydrofuran (THF) solution for the absorption spectra (**Figure 1c,d**). The PL emission of Te and Pe can be observed from the doped crystals of BSB-Me:Te and BSB-Me:Pe (**Figure 1c**) and there is strong spectra overlap between the PL of BSB-Me and the absorption of the Te and Pe (**Figure 1d**), which indicates efficient energy transfer from the donor BSB-Me to the acceptors of Te and Pe at the doping concentration of 8%.<sup>[24–26]</sup> And the photoluminescence quantum yield (PLQY) of pure BSB-Me, BSB-Me:Te, and BSB-Me:Pe crystals shown in the **Figure 1b** can reach up to  $90 \pm 4\%$ ,  $75 \pm 4\%$ , and  $49 \pm 4\%$ , respectively.

### 2.2. Characteristics of the Organic Single-Crystal-Based OLEDs

#### 2.2.1. Single-Crystal-Based OLEDs with the Multilayered Structure

Both anode and cathode of device can be directly deposited onto the opposite surface of the organic single crystals by thermal evaporation based on the simple and nondestructive method of template stripping, enhancing carrier injection by an improved contact between crystals and electrodes.<sup>[22,23]</sup> Au and Ca/Ag are used as electrodes for the hole and electron injection by considering the highest occupied molecular orbital (HOMO) and the lowest unoccupied molecular orbital (LUMO) levels of BSB-Me (5.6 and 2.7 eV, respectively),<sup>[22,27]</sup> as shown in **Figure 2a**. Since the HOMO energy level of BSB-Me (5.6 eV) is much higher

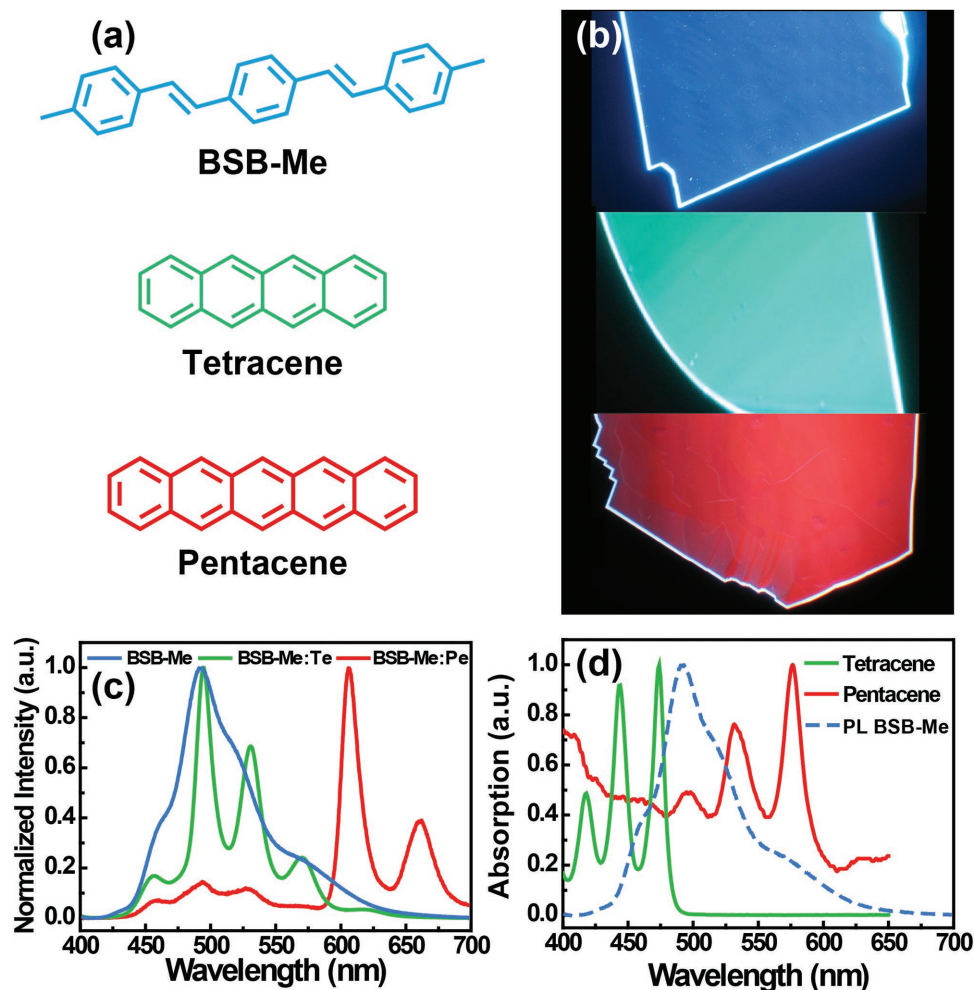


**Figure 1.** a) Chemical structure of BSB-Me and tetracene and pentacene. b) The top-view photographs of BSB-Me, BSB-Me:Te, and BSB-Me:Pe organic crystals under UV-light irradiation by a fluorescence optical microscope. c) PL spectra of BSB-Me, BSB-Me:Te, and BSB-Me:Pe crystals. d) Absorption spectra of tetracene and pentacene in THF solution (PL spectra of BSB-Me is inset to illustrate the overlap).

than the work function of Au (5.1 eV), a high hole-injection barrier ( $\approx 0.5$  eV) at anode will form at the interface and give rise to higher turn-on voltage of device. To lower the turn-on voltage, high work function anode is needed to match the deep HOMO energy level of host material, allowing holes freely injecting to the crystal emissive layer. Here, we use anode buffer layer consisting of the transition metal oxide to further enhance the work function of anode, similar to their roles of modifying the work function of graphene and indium tin oxide (ITO) electrodes in organic electronics.<sup>[28–35]</sup> A transition metal oxide interface layer, MoO<sub>3</sub> (5.3 eV), is subsequently deposited by thermal evaporation on top of the Au electrode (Figure 2b).<sup>[36,37]</sup> This anode buffer layer will provide a work function gradient and thus enable holes to be injected efficiently to the crystal. In conventional OLED structure, electron-transporting/hole-blocking layers are also used between the emissive layer and cathode and have a strong effect on device performance. Then 2,2',2''-(1,3,5-benzinetriyl)-tris(1-phenyl-1-H-benzimidazole) (TPBi) is employed as both electron-transporting layer and hole-blocking layer. And Ca/Ag cathode completes the whole device structure, as shown in Figure 2a. The HOMO and LUMO of

TPBi are 6.1 and 2.8 eV, respectively.<sup>[31,32,38]</sup> The LUMO energy level of TPBi is well aligned with BSB-Me and lower than the work function of Ca (2.9 eV), so better electron injection into the emissive layer through TPBi is expected. And the HOMO of TPBi is lower than that of BSB-Me which will effectively block hole transport, making exciton recombination in the emissive layer of the crystal. The interface modified materials used in devices, MoO<sub>3</sub> and TPBi, are expected to enhance carrier injection and improve charge carrier balance.

A series of BSB-Me crystal-based OLEDs are fabricated based on template stripping method, including single-layered device with a simple structure of Au/BSB-Me/Ca/Ag, double-layered device with an Au/MoO<sub>3</sub>/BSB-Me/Ca/Ag structure (Figure S2a,b, Supporting Information), and multilayered device with Au/MoO<sub>3</sub>/BSB-Me/TPBi/Ca/Ag (Figure 2a). The detail fabrication steps for multilayered single-crystal-based OLEDs have been described accordingly in the Experimental Section as shown in Figure 2b. Here, the thickness of BSB-Me crystals is controlled to be around 350 nm in devices. First, we measure the current–voltage characteristics of the three different devices (Figure 3a). The single-layered device shows

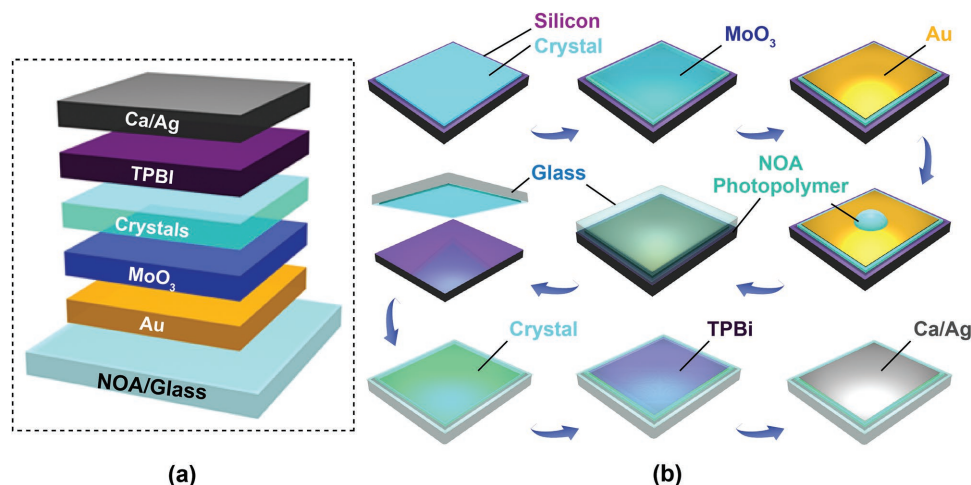


**Figure 2.** a) The single-crystal-based OLEDs with a multilayered structure of Au/MoO<sub>3</sub>/crystal/TPBi/Ca/Ag. b) Schematic illustration of fabrication steps of template stripping technique for the single-crystal-based OLEDs.

a significant low current density and high turn-on voltage of 14 V due to the high energy barrier for the carrier injection. When MoO<sub>3</sub> is used, double-layered and multilayered devices both exhibit a significantly lower turn-on voltage of 4 V, suggesting that, with its high work function lying around 5.3 eV which is very close to the HOMO of BSB-Me, MoO<sub>3</sub> on top of Au anode serves as an excellent anode interface layer for efficient hole injection into BSB-Me crystal.<sup>[36,37]</sup> The luminance–current density characteristics in Figure 3b show that the multilayered device achieve a significant improvement in

luminance compared to single and double-layered devices with a maximum luminance of 66 cd m<sup>-2</sup> at 950 mA cm<sup>-2</sup>, respectively. The significant improvement is also observed in the current efficiency of the multilayered device, and the maximum efficiency of 0.0246 cd A<sup>-1</sup> at 4 mA cm<sup>-2</sup> is obtained (Figure 3c). While, the maximum efficiency of the single and double-layered devices are 0.0017 and 0.0034 cd A<sup>-1</sup>, respectively. The significant improvement in the luminance and current efficiency of the multilayered device is attributed to the better charge carrier balance by efficient electron transport and hole blocking of the

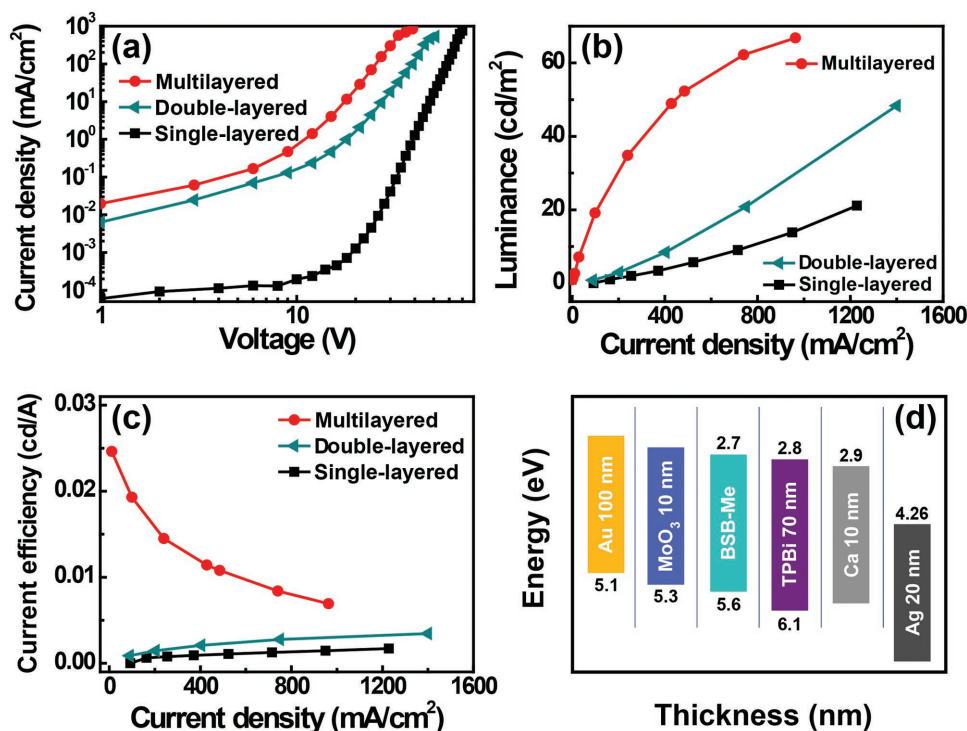


**Figure 3.** EL performance of BSB-Me single-crystal-based OLEDs using three different device structures. a) Voltage–current density, b) current density–luminance, and c) current density–efficiency characteristics of single-crystal-based OLEDs. d) The energy level diagram of the multilayered device, 100 nm Au anode/10 nm MoO<sub>3</sub>/crystal/70 nm TPBi/10 nm Ca and 20 nm Ag cathode.

TPBi layer. Furthermore, the BSB-Me single crystal is placed between two large-bandgap semiconductors in the multilayered structure, confining charge carrier injection and transport for better efficiency.<sup>[39]</sup> The concept is illustrated by the energy level diagram shown in Figure 3d. It is template stripping method that constitutes a major step toward the multilayered structure of organic single-crystal-based OLEDs, by which the modified layers and electrodes can be thermally evaporated on both sides of crystal, tremendously enhancing charge injection and improving charge carrier balance of devices.

As we know, the thickness of the emissive layer has a strong effect on the performance of OLEDs. In order to make high-efficiency and high-brightness single-crystal-based OLEDs, the thickness of the crystals is further decreased. Three BSB-Me crystals with different thicknesses of 353, 291, and 206 nm are employed in the fabrication of single-crystal-based OLEDs in the multilayered device structure. The thickness of crystals is determined by AFM testing. The luminance and current efficiency tend to increase following with the decrease of thickness, obtained from Figure 4a,b. Device with 206 nm BSB-Me crystal shows a maximum current efficiency of 0.16 cd A<sup>-1</sup>, the value is significantly higher than that of the 291 and 353 nm single-crystal-based OLEDs. Considering the poor charge balance in the organic single crystals due to the different hole and electron

mobility, the thinner crystals will give rise to higher exciton recombination efficiency, resulting in sufficient confinement of the excitons in crystals. The achieved highest luminance of the BSB-Me crystal based OLEDs can be up to 200 cd m<sup>-2</sup>.

In addition, the insertion of a hole transport layer of *N,N'*-di(1-naphthyl)-*N,N'*-diphenyl-(1,1'-biphenyl)-4,4'-diamine (NPB) has been attempted to further improve the EL performance of single-crystal-based OLEDs with a structure of Au/MoO<sub>3</sub>/NPB/BSB-Me/TPBi/Ca/Ag. The thickness of the employed BSB-Me crystals is around 200 nm. However, the loose contact problem arises from the addition of NPB because of the low surface energy during the device fabrication. Based on the fabrication of template stripping method, the device will be stripped from the octadecyltrichlorosilane (OTS) modified Si/SiO<sub>2</sub> substrate. During this process, the layer contacting the crystal needs high surface energy, which ensures a compact contact between the crystal and the metal anode. The surface energy of MoO<sub>3</sub> and NPB are about 72.2 and 54.6 mJ m<sup>-2</sup>, respectively, which are evaluated by contact angle measurements (Figure S3a,b, Supporting Information). The surface energy of the transition metal film MoO<sub>3</sub> is much higher than that of the organic film NPB, so the adhesion between the crystal and MoO<sub>3</sub> is better than that with NPB. The luminance of the OLED based on BSB-Me crystal with NPB is much lower than that without NPB. Inhomogeneous light emission also can be seen in the photograph of the OLED based on BSB-Me crystal with NPB (Figure S3c,d, Supporting Information).

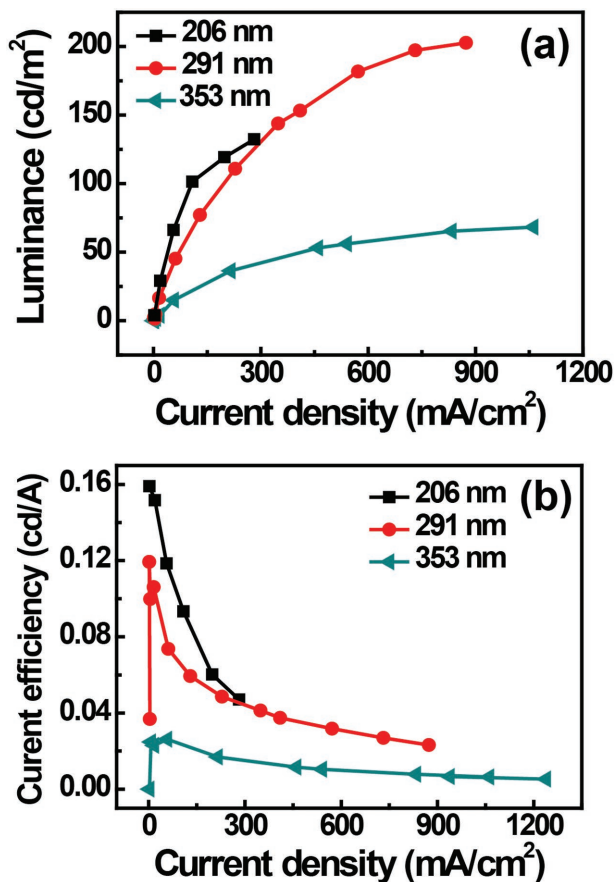


**Figure 4.** Crystal thickness dependent EL performance of the multilayered devices. The thicknesses of the crystals are 206, 291, and 353 nm, respectively. The a) luminance and b) current efficiency as a function of current density.

### 2.2.2. OLEDs with Molecular Doping

The BSB-Me:Te and BSB-Me:Pe crystals at the doping concentration of 8% are applied to the single-crystal-based OLEDs with similar structure of the multilayered device. The thickness of the grown doped crystals keeps as thin as ≈200 nm. The current-voltage characteristics in Figure S4 (Supporting Information) show that OLEDs based on doped and undoped crystals have nearly identical turn-on voltage of 5 V. Figure 5 shows the photographs of the operating devices based on pure BSB-Me, BSB-Me:Te, and BSB-Me:Pe crystals, and uniform light emission from the surface of devices can be observed. Three primary colors' (RGB) EL emission are first time observed from single-crystal-based OLEDs. RGB EL images are captured at a low onset voltage of 5 V and operating voltage of 10 V, respectively. The low turn-on voltage and uniform EL emission also reflect high charge carrier balance and recombination efficiency. The maximum luminance and current efficiency for the BSB-Me:Te and BSB-Me:Pe single-crystal-based OLEDs is 0.72 cd A<sup>-1</sup>, 370 cd cm<sup>-2</sup> and 0.9 cd A<sup>-1</sup>, 820 cd cm<sup>-2</sup>, respectively (Figure 6a,b). The EQE of the OLEDs using BSB-Me, BSB-Me:Te, and BSB-Me:Pe crystals is plotted in Figure 6c. The EQE of the BSB-Me:Te crystal-based OLED is 0.31% at the luminance of 9 cd m<sup>-2</sup>. The method for the calculation of EQE has been demonstrated in our former works.<sup>[22,23]</sup> The EL spectra of single-crystal-based OLEDs in Figure 7a exhibit pure blue, green, and red colors with the major emission peaks at 492, 526, and 610 nm, respectively, indicating high performance of devices based on pure BSB-Me and doped crystals at this doping concentration. The intensity of the RGB EL spectra is increased

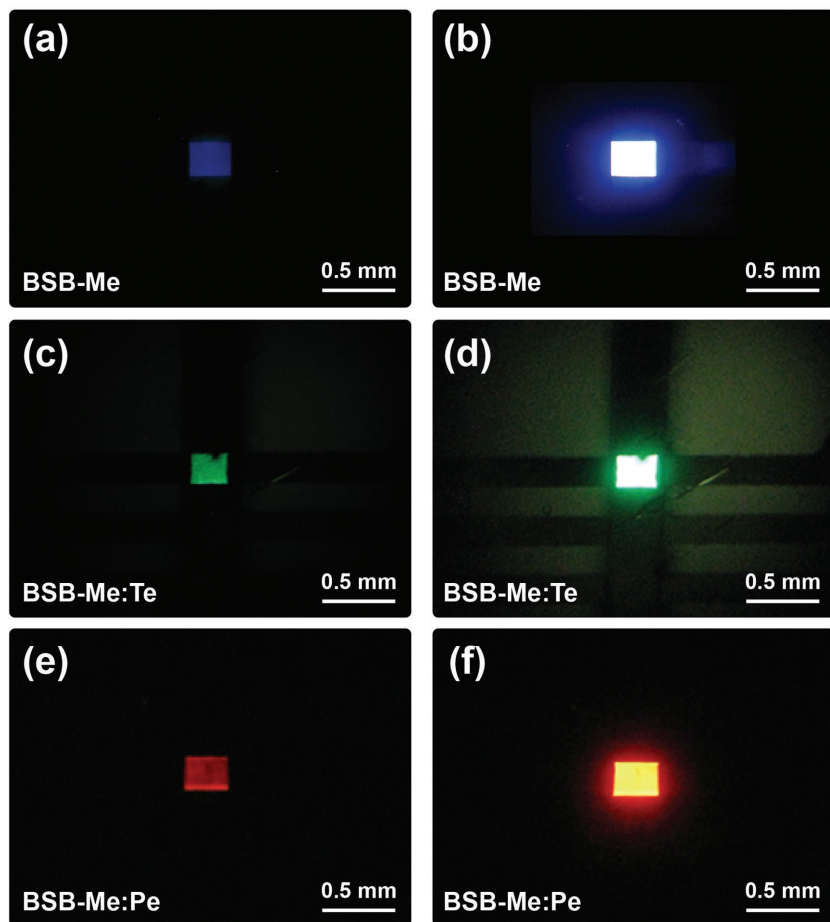


**Figure 5.** Photographs of the operating BSB-Me, BSB-Me:Te, and BSB-Me:Pe single-crystal-based OLEDs at different driving voltage. Single-crystal-based OLEDs driven at the voltage of a,c,e) 5 V and b,d,f) 10 V.

with the increasing current density as shown in Figure S5 (Supporting Information). The chromaticity diagram of these RGB single-crystal-based OLEDs reveals CIE coordinates (0.56, 0.31), (0.23, 0.59), and (0.08, 0.36) (Figure 7b), which are ideal for RGB light emission according to the 1931 CIE coordinate diagram. The remarkable maximum luminance and efficiency we achieved in the doped single-crystal-based OLEDs highly outperform the performance of state-of-the-art organic single crystal-based optoelectronic devices.

Efficient energy transfer from donor BSB-Me to Te and Pe acceptors contribute to the large improvement in luminance and efficiency for the doped single-crystal-based OLEDs. The time-resolved fluorescence of undoped and doped crystals has been investigated to explore the energy transfer in doped crystals by a time-correlated single photon counting (TCSPC) system (Figure S6, Supporting Information). The decay times for BSB-Me, BSB-Me:Te, and BSB-Me:Pe crystals are presented in Table S1 (Supporting Information), by plotting and fitting TCSPC results. As discussed in our former report, the dominating energy transfer process in the doped crystals is Förster energy transfer.<sup>[31]</sup> Then, the rate of energy transfer from a donor to an acceptor  $k_{ET}$  can be calculated from the decay times measured in the absence ( $\tau_0$ ) and presence of acceptor ( $\tau_{DA}$ ) by

the equation:  $k_{ET} = 1/\tau_{DA} - 1/\tau_0$ . Checking the summary of transient PL decay times in Table S1 (Supporting Information), the  $k_{ET}$  is equal to  $1.02 \times 10^{10}$  and  $3.94 \times 10^{10} \text{ s}^{-1}$  for BSB-Me:Te and BSB-Me:Pe crystals at this concentration (25:2). And the calculated energy transfer efficiency is 41% and 72.9%, respectively, given by the equation of  $E = k_{ET}/(1/\tau_0 + k_{ET}) = 1 - \tau_{DA}/\tau_0$ . This efficient energy transfer enables us to fabricate high performance doped single-crystal-based OLEDs. The energy transfer efficiency of BSB-Me:Pe crystals is higher than that of the BSB-Me:Te, which may contribute to the higher luminance and current efficiency for the BSB-Me:Pe single-crystal-based OLEDs. On the other hand, the LUMO levels of Te and Pe molecules (2.85 and 3.2 eV, respectively) are located below that of BSB-Me (2.7 eV), and HOMO levels of Te and Pe (5.4 and 5.0 eV, respectively) lie above that of BSB-Me (5.6 eV), indicating that both Te and Pe molecules act as electron and hole trapping sites.<sup>[11,29]</sup> In order to clarify the effect of doping molecules on the charge carrier transport properties, the time-of-flight (TOF) measurements are used to investigate the carrier mobility of undoped and doped crystals along the *c*-axis of crystal. The devices used for the TOF measurements are based on a structure of Au/crystal/Ca/Ag with an active area of  $500 \times 500 \mu\text{m}^2$ . And the measured TOF transient photocurrent spectra of holes and electrons for pure BSB-Me, BSB-Me:Te, and BSB-Me:Pe crystals are shown in Figure S7 (Supporting Information).

<sup>[19,40]</sup> The calculated hole mobility values of pure BSB-Me, BSB-Me:Te, and BSB-Me:Pe crystals are about  $0.542 \times 10^{-3}$ ,  $0.163 \times 10^{-3}$ , and  $0.203 \times 10^{-3} \text{ cm}^2 \text{ V}^{-1} \text{ s}^{-1}$  for *c*-axis, respectively. And electron mobility values are about  $0.48 \times 10^{-3}$ ,  $0.144 \times 10^{-3}$ , and  $0.192 \times 10^{-3} \text{ cm}^2 \text{ V}^{-1} \text{ s}^{-1}$ , respectively. The measured hole and electron mobility of BSB-Me:Te and BSB-Me:Pe crystals are slightly lower than that of pure BSB-Me, indicating that the tetracene and pentacene molecules dispersed in a BSB-Me host crystal lattice will act as charge trapping sites. This would lead to direct exciton formation at the dopant molecules and significantly improved EL efficiency.

The relatively comparable table for comparing the EL performance of the reported organic single crystal-based OLEDs and OLEFETs has been summarized (Table 1). Our previous works only resolve the contact problem by the method of template stripping, and both electrodes can be directly thermally evaporated onto the opposite surface of organic single crystals to enhance the carrier injection.<sup>[22,23]</sup> The single-crystal-based OLEDs exhibit uniform light-emission with a maximum luminance of  $16.87 \text{ cd m}^{-2}$  by the improved contact between crystal and electrodes. In this work, we overcome the major problems of unbalanced carrier transport and mismatched work function by using the multilayered structure in single-crystal-based

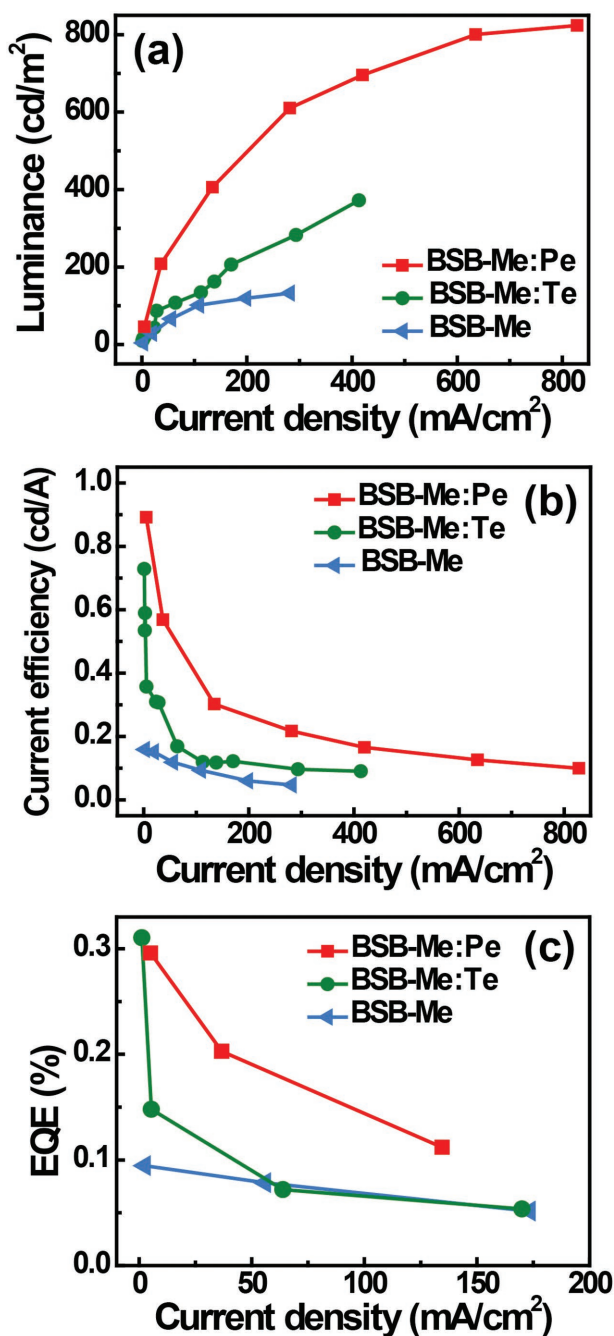


**Figure 6.** EL performance of BSB-Me, BSB-Me:Te, and BSB-Me:Pe single-crystal-based OLEDs. a) Current density–luminance, b) current density–efficiency, and c) current density–EQE characteristics of single-crystal-based OLEDs.

OLEDs with anodic interfacial modification and electron-transport layers. The multilayered structure can enhance the charge injection and balance hole and electron transport in recombination zone of the single-crystal-based OLEDs. However, the current efficiency and luminance of devices are still low, compared to the conventional amorphous film OLEDs. It is thought that the low EL performance arises for the emitting dipole orientation and the thick crystal layer >200 nm. The thick crystal

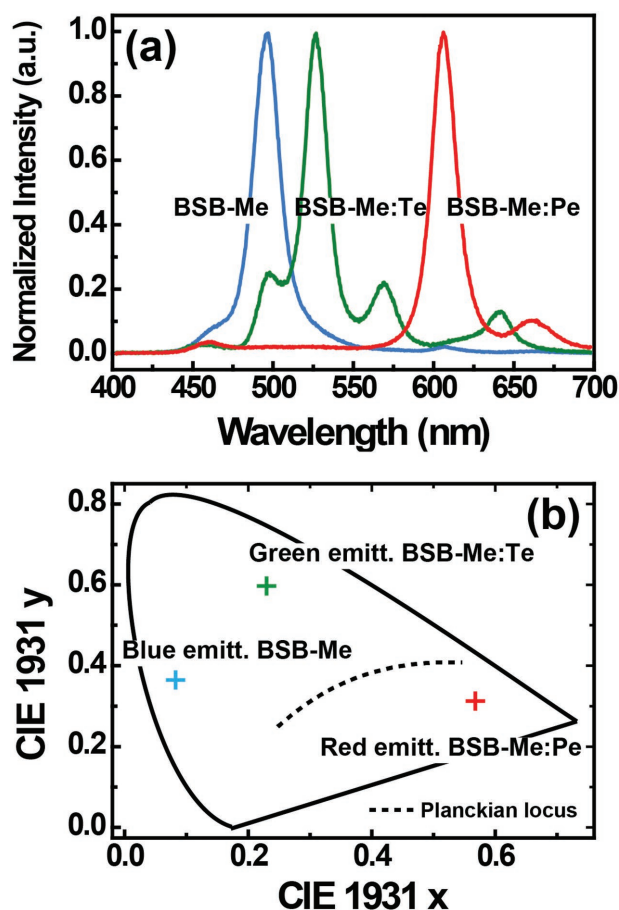


**Figure 7.** a) Three primary colors of EL spectra from BSB-Me, BSB-Me:Te, and BSB-Me:Pe single-crystal-based OLEDs. b) The corresponding 1931 CIE coordinate diagram of blue, green, and red light emission with CIE coordinates of (0.56, 0.31), (0.23, 0.59), and (0.08, 0.36), respectively.

would cause long carrier transport distance which effectively decreases the efficiency of device. And the orientation of emitting dipoles is one of the most important factors of material which influence outcoupling efficiency along with the refractive indices of the consisting materials.<sup>[44]</sup> Recently, Kim and his

**Table 1.** Comparison of EL performance of the reported organic single crystal-based OLEDs and OLEFETs.

Crystal materials	Device type	Luminance [cd m <sup>-2</sup> ]	Current efficiency [cd A <sup>-1</sup> ]	EQE [%]	Ref.
BP1T + AC5-CF <sub>3</sub>	OLEFET	[-]	[-]	0.045	[13]
AC'7	OLEFET	[-]	[-]	3.7 × 10 <sup>-4</sup>	[41]
Tetracene	OLEFET	[-]	[-]	0.03	[42]
Rubrene	OLEFET	[-]	[-]	0.015	[42]
P5V4	OLEFET	[-]	[-]	0.1	[43]
BSB-Me	OLED	7.32	[-]	0.001	[22]
BP2T	OLED	16.87	[-]	0.001	[22]
BP3T	OLED	5	[-]	[-]	[23]
Pentacene doped BSB-Me	OLED	820	0.9	0.31	Present work

co-workers demonstrate a type of OLEDs based on a series of thermal evaporated Pt(II) bis(3-(trifluoromethyl)-5-(2-pyridyl)-pyrazolate) (Pt(fppz)<sub>2</sub>) polycrystalline materials with extremely high horizontal transition dipole ratio of 93% and high maximum EQE of 38.8%.<sup>[44]</sup> But, the molecules in single crystal of BSB-Me exhibit a herringbone packing motif and the long axis of the molecules inclines to the crystal z-axis which would hinder light outcoupling in the crystal layer and induce low EL performance. We expect that the maximum current efficiency, luminance, and EQE can be improved further by decreasing the thickness of crystal layer ≈30 nm and optimizing the device with perfectly oriented single crystal material.

### 3. Conclusion

In summary, we have achieved high luminance and current efficiency in OLEDs based on organic single crystals by modifying interfaces between electrodes and crystals with the multilayered structure. Highly efficient three primary color EL emissions from the single-crystal-based OLEDs have been realized by the multilayered structure and molecular doping technique. The remarkable device performances increase the feasibility of applying the organic single crystals in organic optoelectronic devices by overcoming the major drawbacks of inefficient charge injection and low recombination efficiency of the crystals. This is an important step toward high-performance organic single crystal-based optoelectronic devices for practical lighting and display applications and might be advantageous for the realization of electrically driven organic lasers.

### 4. Experimental Section

**Preparation of Organic Single Crystals:** BSB-Me, Te, and Pe powders were purchased from Tokyo Chemical Industry Co., Ltd. After the Te (or Pe) was uniformly mixed together, the mixture would be placed in a horizontal tube furnace with two heating zones under a flow of pure argon gas. The sublimation and crystallization temperatures for crystal growth were set to 270 and 240 °C. And the temperature conditions were almost the same for pure BSB-Me, BSB-Me:Te, and BSB-Me:Pe. Because the sublimation and crystallization temperature of these compounds are almost the same, the doped crystals can be successfully obtained. In order to get ultrathin crystals, the growth condition had been changed by increasing gas flow rate and short of growing time. In addition, the crystals were grown to be millimeter-scale to ensure that the size was suitable to the metal mask used in the fabrication of devices. So the millimeter-scale crystal was bound to increase the thickness of the crystals. And before the crystals transferred to the OTS modified Si/SiO<sub>2</sub> substrate, the crystals were selected with a thickness above 200 nm, avoiding curling up when touched by the tweezers.

**Device Fabrication:** The multilayered structure devices were fabricated based on template stripping method according to the previous reports, as shown in Figure 2b.<sup>[22,23]</sup> Single crystals were transferred onto the OTS modified Si/SiO<sub>2</sub> substrate after growth. Then, based on the structure of multilayered device, 10 nm MoO<sub>3</sub> and 100 nm thick Au anode were deposited onto the organic crystal by thermal evaporation, respectively. A droplet of NOA 63 photoresist (Norland) was placed on the device and compressed by a piece of glass. The photoresist would spread to the edge and cover the whole glass. Then, the device was transported under a UV lamp of 250 mW with a protection distance of about 15 cm away from the lamp source. The ambient temperature of device was about 50–80 °C which was much lower than the growing temperature

of ≈270 °C. Therefore, no damage would be brought to the organic device during the UV curing process. After exposed to the UV-light, the photoresist would be cured and peeled off from Si/SiO<sub>2</sub> substrate with device and the device was transferred to the glass substrate. Finally, 70 nm TPBi and a 10 nm Ca and 20 nm Ag cathode were, respectively, evaporated onto the template-stripped organic crystal. The thermal evaporation rate could be controlled to be 1 Å s<sup>-1</sup> at pressure of 5 × 10<sup>-4</sup> Pa. The active area of the device was determined by the metal mask of 200 × 300 μm<sup>2</sup>.

**Characterizations and Measurements:** The top-view photographs of crystals were observed under 405 nm laser excitation by using widefield fluorescence microscopy on BK-FL4 fluorescence microscope. The emission spectra were detected by the optical fiber and dispersed to the spectrometer connected with charge coupled device detector (Andor iDus). The PLQY was measured by using an integrating sphere (C-701, Labsphere Inc.) with an excitation source of 405 nm Ocean Optics LLS-LED, and the laser light was introduced into the sphere through the optical fiber. The TCSPC system equipped with a 379 nm picosecond diode laser (Edinburgh Instruments EPL375, repetition rate 20 MHz) was used to excite the sample. And the emission was detected by a photomultiplier tube (Hamamatsu H5783p) and a TCSPC board (Becker & Hickel, SPC-130). The crystal thicknesses were measured by AFM (Digital Instruments Nanoscope IIIA) in tapping mode. And the surface morphology and root mean square roughness of crystals were measured in contact mode. The current density–voltage characteristics of the devices were measured by a Keithley 2400 programmable voltage–current source. And the brightness of the single-crystal-based OLEDs was detected by the Photo Research PR-655 spectrophotometer.

### Supporting Information

Supporting Information is available from the Wiley Online Library or from the author.

### Acknowledgements

The authors gratefully acknowledge the financial support from the 973 Project (2013CBA01700), the National Natural Science Foundation Program of China (Grant Nos. 61322402, 61604018, 61675085, 61605065, 61505065 and 61590930), the Jilin Provincial Science and Technology Program (20160520101JH), and the China Postdoctoral Science Foundation (2015M581377).

Received: September 8, 2016

Revised: December 26, 2016

Published online: February 15, 2017

- [1] J. H. Burroughes, D. D. C. Bradley, A. R. Brown, R. N. Marks, K. Mackay, R. H. Friend, P. L. Burns, A. B. Holmes, *Nature* **1990**, 347, 539.
- [2] M. A. Baldo, D. F. O'Brien, Y. You, A. Shoustikov, S. Sibley, M. E. Thompson, S. R. Forrest, *Nature* **1998**, 395, 151.
- [3] R. H. Friend, R. W. Gymer, A. B. Holmes, J. H. Burroughes, R. N. Marks, C. Taliani, D. D. C. Bradley, D. A. Dos Santos, J. L. Brédas, M. Lögdlund, W. R. Salaneck, *Nature* **1999**, 397, 121.
- [4] Z. Shen, P. E. Burrows, V. Bulovic, S. R. Forrest, M. E. Thompson, *Science* **1997**, 276, 2009.
- [5] C. D. Müller, A. Falcou, N. Reckefuss, M. Rojahn, V. Wiederhirn, P. Rudati, H. Frohne, O. Nuyken, H. Becker, K. Meerholz, *Nature* **2003**, 421, 829.
- [6] S. R. Forrest, *Nature* **2004**, 428, 911.

- [7] B. W. D'Andrade, S. R. Forrest, *Adv. Mater.* **2004**, *16*, 624.
- [8] Y. Sun, S. R. Forrest, *Nat. Photonics* **2008**, *2*, 483.
- [9] S. Reineke, F. Lindner, G. Schwartz, N. Seidler, K. Walzer, B. Lüssem, K. Leo, *Nature* **2009**, *459*, 234.
- [10] C. W. Tang, S. A. VanSlyke, *Appl. Phys. Lett.* **1987**, *51*, 913.
- [11] H. Nakanotani, M. Saito, H. Nakamura, C. Adachi, *Adv. Funct. Mater.* **2010**, *20*, 1610.
- [12] R. Kabe, H. Nakanotani, T. Sakanoue, M. Yahiro, C. Adachi, *Adv. Mater.* **2009**, *21*, 4034.
- [13] K. Kajiwara, K. Terasaki, T. Yamao, S. Hotta, *Adv. Funct. Mater.* **2011**, *21*, 2854.
- [14] K. Sawabe, M. Imakawa, M. Nakano, T. Yamao, S. Hotta, Y. Iwasa, T. Takenobu, *Adv. Mater.* **2012**, *24*, 6141.
- [15] S. Z. Bisri, T. Takenobu, Y. Yomogida, H. Shimotani, T. Yamao, S. Hotta, Y. Iwasa, *Adv. Funct. Mater.* **2009**, *19*, 1728.
- [16] C. Goldmann, S. Haas, C. Krellner, K. P. Pernstich, D. J. Gundlach, B. Batlogg, *J. Appl. Phys.* **2004**, *96*, 2080.
- [17] M. Yamagishi, J. Takeya, Y. Tominari, Y. Nakazawa, T. Kuroda, S. Ikehata, M. Uno, T. Nishikawa, T. Kawase, *Appl. Phys. Lett.* **2007**, *90*, 182117.
- [18] M. Ichikawa, K. Nakamura, M. Inoue, H. Mishima, T. Haritani, R. Hibino, T. Koyama, Y. Taniguchi, *Appl. Phys. Lett.* **2005**, *87*, 221113.
- [19] X. Li, Y. Xu, F. Li, Y. Ma, *Org. Electron.* **2012**, *13*, 762.
- [20] H. Nakanotani, C. Adachi, *Appl. Phys. Lett.* **2010**, *96*, 053301.
- [21] H. Yanagi, T. Morikawa, S. Hotta, *Appl. Phys. Lett.* **2002**, *81*, 1512.
- [22] R. Ding, J. Feng, X. L. Zhang, W. Zhou, H. H. Fang, Y. F. Liu, Q. D. Chen, H. Y. Wang, H. B. Sun, *Adv. Funct. Mater.* **2014**, *24*, 7085.
- [23] R. Ding, J. Feng, W. Zhou, X. L. Zhang, H. H. Fang, T. Yang, H. Y. Wang, S. Hotta, H. B. Sun, *Sci. Rep.* **2015**, *5*, 12445.
- [24] H. Nakanotani, C. Adachi, *Adv. Opt. Mater.* **2013**, *1*, 422.
- [25] H. Wang, F. Li, B. R. Gao, Z. Q. Xie, S. J. Liu, C. L. Wang, D. H. Hu, F. Z. Shen, Y. X. Xu, H. Shang, Q. D. Chen, Y. G. Ma, H. B. Sun, *Cryst. Growth Des.* **2009**, *9*, 4945.
- [26] H. H. Fang, S. Y. Lu, L. Wang, R. Ding, H. Y. Wang, J. Feng, Q. D. Cheng, H. B. Sun, *Org. Electron.* **2013**, *14*, 389.
- [27] H. Nakanotani, R. Kabe, M. Yahiro, T. Takenobu, Y. Iwasa, C. Adachi, *Appl. Phys. Express* **2008**, *1*, 091801.
- [28] H. Nakanotani, H. Kakizoe, C. Adachi, *Solid State Commun.* **2011**, *151*, 93.
- [29] M. T. Greiner, M. G. Helander, W. M. Tang, Z. B. Wang, J. Qiu, Z. H. Lu, *Nat. Mater.* **2012**, *11*, 76.
- [30] N. Li, S. Oida, G. S. Tulevski, S. H. Han, J. B. Hannon, D. K. Sadana, T. C. Chen, *Nat. Commun.* **2013**, *4*, 2297.
- [31] C. Adachi, M. A. Baldo, S. R. Forrest, S. Lamansky, M. E. Thompson, R. C. Kwong, *Appl. Phys. Lett.* **2001**, *78*, 1622.
- [32] S. C. Lo, N. A. H. Male, J. P. J. Markham, S. W. Magennis, P. L. Burn, O. V. Salata, I. D. W. Samuel, *Adv. Mater.* **2002**, *14*, 13.
- [33] U. Kitamura, E. Shikoh, K. Sawabe, T. Takenobu, M. Shiraishi, *Appl. Phys. Lett.* **2012**, *101*, 073501.
- [34] N. Li, B. E. Lassiter, R. R. Lunt, G. D. Wei, S. R. Forrest, *Appl. Phys. Lett.* **2009**, *94*, 023307.
- [35] D. Y. Kim, J. Subbiah, G. Sarasqueta, F. So, H. J. Ding, Irgan, Y. L. Gao, *Appl. Phys. Lett.* **2009**, *95*, 093304.
- [36] F. J. Zhang, D. W. Zhao, Z. L. Zhuo, H. Wang, Z. Xu, Y. S. Wang, *Sol. Energy Mater. Sol. Cells* **2010**, *94*, 2416.
- [37] V. Shrotriya, G. Li, Y. Yao, C.-W. Chu, Y. Yang, *Appl. Phys. Lett.* **2006**, *88*, 073508.
- [38] S. H. Kim, J. Jang, *Appl. Phys. Lett.* **2007**, *91*, 083511.
- [39] T.-H. Han, Y. B. Lee, M.-R. Choi, S.-H. Woo, S.-H. Bae, B. H. Hong, J.-H. Ahn, T.-W. Lee, *Nat. Photonics* **2012**, *6*, 105.
- [40] H. Wang, F. Li, I. Ravia, B. Gao, Y. Li, V. Medvedev, H. Sun, N. Tessler, Y. Ma, *Adv. Funct. Mater.* **2011**, *21*, 3770.
- [41] T. Yamao, Y. Sakurai, K. Terasaki, Y. Shimizu, H. Jinnai, S. Hotta, *Adv. Mater.* **2010**, *22*, 3708.
- [42] T. Takenobu, S. Z. Bisri, T. Takahashi, M. Yahiro, C. Adachi, Y. Iwasa, *Phys. Rev. Lett.* **2008**, *100*, 066601.
- [43] H. Nakanotani, M. Saito, H. Nakamura, C. Adachi, *Appl. Phys. Lett.* **2009**, *95*, 103307.
- [44] K. Kim, J. Liao, S. W. Lee, B. Sim, C. Moon, G. Lee, H. J. Kim, Y. Chi, J. Kim, *Adv. Mater.* **2016**, *28*, 2526.